Atmos. Meas. Tech., 16, 3679–3692, 2023
https://doi.org/10.5194/amt-16-3679-2023

Atmospheric Measurement Techniques
Open Access
EGU

A new smog chamber system for atmospheric multiphase chemistry study: design and characterization

Taomou Zong[1], Zhijun Wu[1,2], Junrui Wang[1,3], Kai Bi[4], Wenxu Fang[1], Yanrong Yang[1], Xuena Yu[1], Zhier Bao[5], Xiangxinyue Meng[1], Yuheng Zhang[1], Song Guo[1,2], Yang Chen[5], Chunshan Liu[6], Yue Zhang[7], Shao-Meng Li[1], and Min Hu[1,2]

[1]State Key Joint Laboratory of Environmental Simulation and Pollution Control, College of Environmental Sciences and Engineering, Peking University, Beijing 100871, China
[2]Collaborative Innovation Center of Atmospheric Environment and Equipment Technology, Nanjing University of Information Science and Technology, Nanjing 210044, China
[3]Laboratory of Atmospheric Observation Supersite, School of Environment and Energy, Peking University Shenzhen Graduate School, Shenzhen 518055, China
[4]Beijing Key Laboratory of Cloud, Precipitation and Atmospheric Water Resources, Beijing Weather Modification Center, Beijing 100089, China
[5]Research Center for Atmospheric Environment, Chongqing Institute of Green and Intelligent Technology, Chinese Academy of Sciences, Chongqing 400714, China
[6]Beijing Convenient Environmental Tech Co. Ltd., Beijing 101115, China
[7]Department of Atmospheric Sciences, Texas A&M University, College Station, TX 77843, United States

Correspondence: Zhijun Wu (zhijunwu@pku.edu.cn)

Received: 17 February 2023 – Discussion started: 18 April 2023
Revised: 7 June 2023 – Accepted: 16 June 2023 – Published: 8 August 2023

Abstract. Multiphase chemistry is an important pathway for the formation of secondary organic aerosols (SOAs) in the atmosphere. In this study, an indoor 2 m^3 Teflon chamber system (Aerosol multIphase chemistry Research chamber, AIR) was developed and characterized to specifically simulate atmospheric multiphase chemistry processes. The temperature and humidity controls, diurnal variation simulation, and seed particle generation unit in this chamber system were designed to meet the needs of simulating multiphase atmospheric chemical reactions. The AIR chamber is able to accurately control temperature (2.5–31 $\pm$ 0.15 °C) and relative humidity (RH $<$ 2 %–$>$ 95 % $\pm$ 0.75 %) over a relatively broad range. In addition, an RH regulation module inside the chamber was designed to simulate the diurnal variation of ambient atmospheric RH. The aerosol generation unit is able to generate pre-deliquescent seed particles with an organic coating across a wide range of phase states or morphologies. The organic coating thickness of the aerosols within the chamber can be precisely controlled through adjusting the condensation temperature, further helping to elucidate the roles of seed particles in multiphase chemical reactions. The inner walls of the AIR chamber are passivated to reduce the wall loss rates of reactive gases. Yield experiments of α-pinene ozonolysis with and without seed particles combined with a box model simulation demonstrate the high-quality performance of secondary aerosol formation simulation using the AIR chamber.

1 Introduction

A smog chamber is a mainstream tool in chemical laboratory studies to simulate the formation and evolution of air pollutants (Batchvarova et al., 2006; Chen and Lelevkin, 2006; Kolev and Grigorieva, 2006; Mocanu et al., 2006; Tolkacheva, 2006) and reveal the parameterization or mechanisms of atmospheric processes (Wenger, 2006; Olariu et al., 2006; Bejan et al., 2006; Mellouki, 2006; Barnes, 2006; Albu et al., 2006; Carter, 2006; Rudzinski, 2006; Zielinska et al., 2006). Chamber simulations have irreplaceable advantages

over other laboratory methods such as oxidation flow reactors (Kang et al., 2007; Lambe et al., 2015; Corral Arroyo et al., 2018; Cosman and Bertram, 2008) and bulk solution experiments (Brunamonti et al., 2015; Turšič et al., 2003; Pratap et al., 2021; Fleming et al., 2020; Mekic et al., 2019) in tracking atmospheric transformation processes and understanding kinetic processes.

The development of chambers is closely related to advances in atmospheric chemistry research. Starting with studies of photochemical smog in Los Angeles in the 1940s (Haagensmit, 1952) and continuing to the 1970s, chambers were primarily designed to study the formation of ozone (Akimoto et al., 1979; Carter et al., 1982) as well as the chemistry of volatile organic compounds (VOCs) and NO_x (Morriss et al., 1957) in the atmospheric boundary layer. With the development of submicron particle measurement techniques, chambers were further used in secondary organic aerosol (SOA) formation studies from the 1980s, leading to numerous important scientific discoveries (Hidy, 2019; Odum et al., 1996, 1997; Griffin et al., 1999; Paulsen et al., 2005; Rollins et al., 2009; Hu et al., 2014; Wang et al., 2014). Since the beginning of the 21st century, many chambers have been built or upgraded to address integrated atmospheric scientific questions, including $PM_{2.5}$ pollution (Johnson et al., 2004; Hallquist et al., 2009; Hurley et al., 2001), reaction kinetic parameters, mechanisms of VOC oxidation intermediates (Brauers et al., 2003; Bohn et al., 2005; Ren et al., 2017), and multiphase processes (Warneke and C., 2004; Pöschl and Shiraiwa, 2015; Liu and Abbatt, 2021; Franco et al., 2021).

In recent years, multiphase chemistry has been invoked to explain the bursting growth of particles (Su et al., 2016; Wang et al., 2016; Su et al., 2020) and physicochemical processes of SOA formation under high ionic strength conditions in the atmosphere (Cheng et al., 2015; Su et al., 2020; Liu et al., 2021). Atmospheric multiphase processes can undergo different reaction pathways that are influenced by different environmental conditions (e.g. light, temperature, and relative humidity – RH) and aerosol physicochemical properties including aerosol liquid water content (ALWC), aerosol phase state, and morphology (George and Abbatt, 2010; Davidovits et al., 2011; Abbatt et al., 2012; Ziemann and Atkinson, 2012; Herrmann et al., 2015; Ravishankara, 1997; George et al., 2015; Su et al., 2020). Thus, a precise control of such parameters in a chamber system is vital for simulating atmospheric multiphase chemistry. Different from outdoor chambers (Leone et al., 2010; Stern et al., 1987; Pandis et al., 1991; Johnson et al., 2004; Martin-Reviejo and Wirtz, 2005; Rollins et al., 2009; Peng et al., 2017), indoor chambers are usually equipped with artificial light sources (Cocker et al., 2001a, b; Takekawa et al., 2003; Carter et al., 2005; Paulsen et al., 2005) that can provide controllable irradiation for the simulation of multiphase processes. Compared to large chambers (Brauers et al., 2003; Leone et al., 1985; Pandis et al., 1991), temperature and RH inside small chambers can achieve faster equilibria and provide a more precise simulation of parameters such as diurnal RH change and ALWC (Takekawa et al., 2003; Carter et al., 2005; Paulsen et al., 2005; Wang et al., 2014; Bin Babar et al., 2016), thus improving reproducibility and efficiency when conducting experiments. In addition, small chambers may have the potential for controlling RH change and simulating co-condensation phenomena. Adversely, the wall loss effects are more significant for small chambers (Carter et al., 1982; Carter and Lurmann, 1991; Dodge, 2000). The influence of aerosol phase state on kinetics of gas–particle interactions has received increasing attention (Virtanen et al., 2010; Berkemeier et al., 2016; B. Wang et al., 2015; Reid et al., 2018), and this requires that the phase state of seed particles can be controlled in chamber simulations. A laboratory study using a pre-deliquescence way to control particle phase state has been reported (Faust et al., 2017), providing a feasible way for phase state control. Regarding particle morphology, some chamber-based experimental studies in recent years have preliminarily shown that organic coatings have important effects on the kinetics of aerosol multiphase transformation (Zhou et al., 2019; Zhang et al., 2018, 2019), which deserves more research. As these studies showed evidence that the morphology and phase state of aerosol particles play important roles in the atmospheric multiphase chemistry processes, focused chamber studies on multiphase chemistry require additional steps to control the morphology and phase state of seed particles in chamber design.

In this study, we designed and built a new indoor 2 m^3 Teflon chamber system (Aerosol multIphase process Research chamber, AIR) with a focus on accurately simulating atmospheric multiphase processes. The temperature and RH inside the AIR chamber were precisely controlled to within $\pm 0.15\,^{\circ}C$ and $\pm 0.75\,\%$, respectively. A quantitative manipulation of the RH cycle was designed to simulate the diurnal variations in ambient RH. The seed generation subsystem, including an inorganic particle pre-deliquescence unit and an organic-coating unit, was designed to manipulate the aerosol phase state and organic-coated morphology. A series of experiments were conducted to characterize the spectral distribution and photolysis parameters of light sources, temperature, RH, wall loss behaviours of gas and particles, and particle morphology. Additionally, a series of experiments involving the oxidation of α-pinene with seed particles were conducted in the AIR chamber to demonstrate the effectiveness of the chamber in simulating atmospheric multiphase chemistry. Our results indicate that the AIR chamber system has more precise temperature and RH control capabilities compared to other chambers. Phase state and morphology of seed particles can also be accurately manipulated in advance, which is rare in existing smog chamber systems.

2 Facility

Figure 1 displays the schematic design of the AIR chamber system, and the real picture of the reactor bag and enclosure system are shown in Fig. S1 in the Supplement. The chamber system includes the 2 m^3 fluorinated ethylene propylene (FEP) Teflon film (75 µm, Du Pont, USA, light transmission $\geq 93\,\%$) reactor and the associated temperature and RH control, artificial light sources, zero-air injection and humidification, gaseous/liquid precursor injection, seed aerosol generation, and the instrument-optional detection components. To achieve a precise control of thermodynamic parameters and aerosol morphology when simulating atmospheric multiphase chemistry processes, the temperature inside the reactor is precisely controlled to within $\pm 0.15\,°C$. An RH regulation module is designed and built to simulate the ambient RH diurnal variation, which is capable of changing the RH in the reactor at a timescale of half an hour. In addition, a predeliquescing device and a coating device are custom-built to be coupled to the seed aerosol generation component for manipulating the phase state (metastable aqueous or solid) and core–shell morphology (1 %–12 % shell thickness) of seed aerosols. The detailed description of each system is shown in Sect. 2.1–2.4.

2.1 The reactor and enclosure

The Teflon reactor is a 2 m^3 horizontal cylinder (1.2 m in diameter, 1.8 m in length). It is fixed on a stainless-steel frame with four ridges firmly adhered on the Teflon air bag (Fig. S1) so that the variable volume of the reactor during sampling is adequate (this chamber system is designed to operate in batch mode). As to each circle side of the cylinder, three stainless-steel tubes are threaded through the Teflon film to act as the inlets (for injecting seeds and liquid phase precursors) or sampling outlets for the detection system, respectively. The interface between each tube and the film is sealed by a Teflon flange and a perfluorinated O-ring. At the bottom inside the reactor, two magnetic-levitation fans (patent number: 2019213329392, Beijing Convenient Environmental Tech Co. Ltd.) are equipped, with four speed levels (1000, 1350, 1700, 2000 rpm). A temperature and RH sensor (HMP110, Vaisala, Finland) and a differential pressure sensor (MSX-W10-PA-LCD, Dwyer, America) are also equipped at the bottom inside the reactor.

The rectangular enclosure ($2.4 \times 1.6 \times 2.3$ m, L, W, H) of the reactor is temperature-controlled by a circulation system. The indoor air is introduced from the top of the enclosure and exhausts through the bottom. The chiller power is constant, while the heating power is controlled through a proportional–integral–derivative (PID) feedback. Forty black lights (1.2 m, 40 W, Bulb-T12, GE, USA) are fixed on the inner wall of the enclosure as light sources for atmospheric process simulation. The number and position of these lights in work can be controlled by the system computer so that the light intensity can be variable in experiments. Specular-insulated material (SUS304, stainless steel, 8 K, mirror plate) is used as the enclosure inner wall so that the irradiation inside the reactor can be homogeneous. One side of the enclosure is a double door for entering and reactor maintenance.

2.2 Cleaning and humidifying system

The background gas in the reactor is from the indoor air. An air compressor (FOHUR, FH-50L) compresses the indoor air into a zero-air generator (Aadco, 737-14-A-CH4-240) for purification, removing airborne contaminants such as particulate matters, hydrocarbons, water vapour, NO_x, O_3, and SO_2 to produce zero air (RH can be dried to $< 2\,\%$, and the background concentrations of other contaminants are displayed in Table S2). Then, with the control of a mass flow controller (MFC, HORIBAMETRON, S4832/HMT), zero air is fed into the reactor through a 1/2 in. stainless-steel tube (sealed at the bottom interface by a 304 stainless-steel flange) at a flow rate of $\leq 50\,L\,min^{-1}$ (to ensure that the cleaning efficiency of the zero-air generator is sufficient), acting as the background gas and cleaning gas for the reactor. At the same time of feeding into the cleaning zero air, a pump beside the chamber system will exhaust the air from the reactor with a flow rate of $20\,L\,min^{-1}$ to accelerate the gas exchange. The positive differential pressure inside the reactor is monitored. When the differential pressure reaches 30 Pa, the MFC will stop the zero-air feed, and when the value falls below 20 Pa, zero-air feed will restart. This is designed to avoid damaging the Teflon film of the reactor during cleaning.

The zero air is also used as humidifying gas. When switching to the humidification mode, the zero air will go into a humidification tank filled with deionized water (Milli-Q, 18 MΩ) switched by a three-way valve, generating humidified zero air. Then, the humidified air flows through a filter (Waterman, HEPA) to remove the water droplet and injects into the reactor to humidify. During the humidifying, the exhaust pump mentioned above keeps working. The flow rate of the humidified zero air ($20–25\,L\,min^{-1}$) is set to be slightly higher than the exhausting rate for fast reaching the target RH inside the reactor.

2.3 Precursor injection system

According to the phase state of precursor reagents, the precursor injection system of this chamber system contains two types. One is used for the injection of gaseous precursors. Standard gas cylinders containing reactive gas (such as SO_2, NO_2, NH_3, and HCHO) inject relevant gaseous precursors into the reactor at a set flow rate and injecting duration under the control of a computer-connected MFC. The oxidant O_3 is produced through the decomposition of O_2 (from a standard O_2 cylinder) exposed to the 185 nm UV light. After flowing through the MFC, the gaseous species enter the reactor via a stainless-steel tube at the bottom of the chamber.

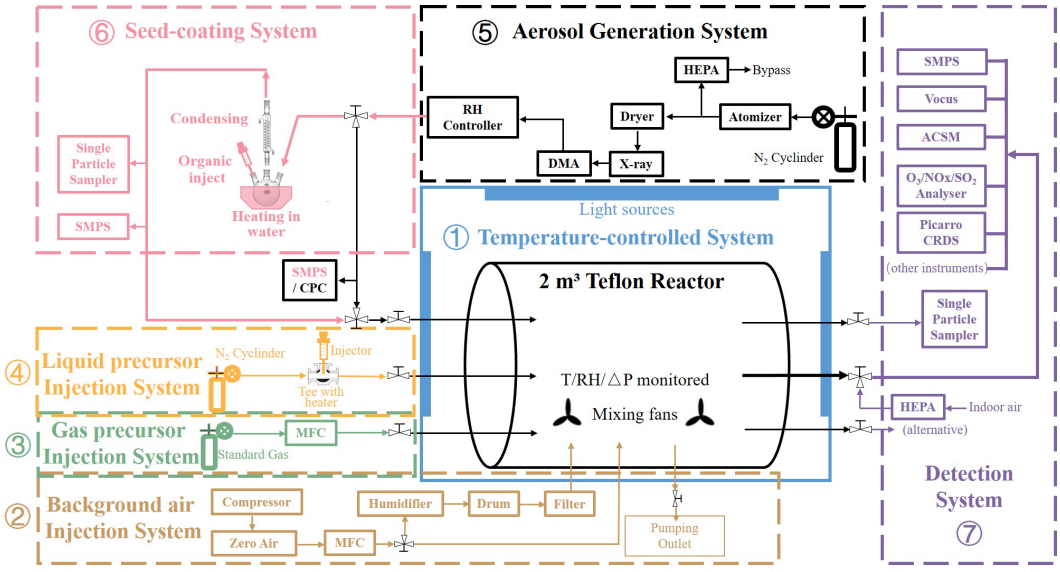

Figure 1. Schematic diagram of the AIR chamber system.

The other type is used for the injection of liquid precursors. Note that the liquid precursors here mean that the species is in liquid phase before being injected into the reactor, but should be gaseous after being injecting into the chamber, such as α-pinene standard solvent. A tee (the inlet on the left side of the chamber, as shown in the "Liquid precursor Injection System" in Fig. 1) is fitted in the pipeline before the liquid precursors entering the reactor, with a 1 mm thick silicone membrane clamped to the right-angled end. The specific amount of the liquid precursors is taken with a microsyringe, penetrating the silicone membrane and slowly injected into the tee. At the same time, pure N_2 is used as the carrier gas to vaporize the liquid precursor and carry it into the reactor under a specific gas cylinder pressure (0.25 MPa). After injection, N_2 is continuously purged for 60 s to ensure that no liquid precursors remain in the pipeline.

2.4 Seed generation system

The seed aerosol generating system is a complex subsystem of the AIR chamber system designed in this study. In addition to the common aerosol generation device, this study couples an RH-controlling device and a coating device to control the phase state and morphology of the seeds for supporting the simulation of atmospheric multiphase processes.

Commonly, the species used to generate the seed particles (typically dissolved inorganic salts such as ammonium sulfate and sodium chloride) are first dissolved in deionized water (Milli-Q, 18 MΩ) and then generate a solution. Then, it is atomized as humid aerosol flow by an atomizer (TSI 3076) with N_2 blowing. Passing through a Nafion tube (PERMA PURE, MD-700-24F-3), the humid flow is dried and forms dry polydisperse seed aerosols. The drying is realized by pumping the air at the outer layer of the Nafion tube to a negative pressure ($\sim$ 20 kPa). It is tested that, within the range of the aerosol generation flow rate ($\leq 3\,\mathrm{L\,min^{-1}}$), the RH of the aerosol flow can be dried to below 30 %. An X-ray neutralizer and differential mobility analyser (DMA, model 3082, TSI, Inc., USA) are optional for selecting monodisperse aerosols from the polydisperse aerosol flow (flow rate ratio of sheath flow to aerosol flow is controlled between 5 : 1 and 10 : 1) to support monodisperse experiments. For polydisperse seeds experiments, the seed generation system can inject seeds into the reactor to the desired amount within a timescale of seconds to several minutes. For monodisperse seed experiments, if large-sized seeds that have a lower number fraction in the generated aerosol population are selected, the timescale will expand to 40–50 min. The appropriate timescale for seed injection can be adjusted by changing the solution concentration and aerosol flow rate.

Besides, an RH controlling device is designed in this study to pre-deliquesce the generated dry seeds that form metastable seed aerosols. As shown in Fig. S9, N_2 is used as the initial gas, which is then divided into two paths: one is the dry N_2 and the other goes through the deionized water (Milli-Q, 18 MΩ, heated to 45 °C) to act as the wet gas. The flow rate of each path is controlled by an MFC (GAS TOOL INSTRUMENT, GT 130MAX). Then the two flows mix into one as the humidifying gas and enter the outer layer of a Nafion semi-permeable tube (PERMA PURE, MD-700-24F-3). The flow with seed aerosols goes through the inner layer of the Nafion tube and is then humidified. The RH of the humidified flow is detected by an RH sensor (HYGROCLIP2, HC2A-S). The two MFCs of each flow path and the RH sensor are connected to a computer and controlled by LabView programming with PID feedback. With the two MFCs adjust-

ing the ratio of the flow rates of the dry and wet flow path, the RH of seed aerosol flow is controlled. This device has been tested to enable rapid changes in RH between 5 % and 90 % within 5 min, and the RH variability can be within ±0.2 %.

In order to investigate the effect of aerosol coating on atmospheric multiphase process, a device is designed in this study to generate a thickness-controlled and species-known coating on the generated dry monodisperse seed aerosols. The constitution of the coating device is shown in Fig. S10. This device consists of a water bath (Changfeng, HW.SY11-KP1), a three-necked flask (250 mL; sizes 19, 24, 19), a condensing glass tube (30 cm, size 24), and a thermostatic bath (BiLon, SC-05B). The organic species (∼ 400 µL) with low volatility (saturated vapour pressure in the order of 10^{-4}–10^{-5} mm Hg at room temperature) used to form coating is set at the bottom of the three-necked flask, which is heated in the water bath to evaporate the organic vapour. The dried seed aerosol flow enters through the side port of the three-necked flask, and then carries the hot organic vapour into the condensing tube (condensing temperature is controlled at 20 °C by the thermostatic bath in this study). Due to the reduced temperature, the saturated vapour pressure of the organic vapour drops, and the organic vapour will preferentially condense on the surface of seed aerosols that form a coating. The coating efficiency can be kept stable within 4 h, which is sufficient to meet the duration of injecting seeds for general experiments.

2.5 Detection system

As shown in Fig. 1, three stainless-steel tubes are fixed on the right side of the reactor to act as sampling outlets. The middle steel tube of them is 3/8 in. in size and acts as the main sampling tube, connected to a 3/8 in. stainless-steel three-way plug valve. One outlet of the plug is attached to a HEPA filter, and the other outlet is attached to the line to sampling instruments. This design allows a quick sampling switch between indoor air and the reactor. The other two stainless-steel tubes are both 1/4 in. and are used as auxiliary sampling outlets (e.g. temporarily collect single particle samples for a few minutes).

A scanning mobility particle sizer (SMPS) system (a DMA, model 3082, and a condensation particle counter – CPC, model 3772, TSI, Inc., USA) and a CPC (model 3750, TSI, Inc., USA) downstream of the seed generation system are the standing instruments for the chamber system, used to measure the particle number size spectrum distribution and particle total number concentration in the reactor, respectively. Other instruments are optional according to the specific research aim, and typically the total sampling flow rate should be lower than 6 L min^{-1}.

The other detection instruments involved in this study include instruments for gaseous species detection (Thermo Scientific gas analyser: model 43i-TLE for SO_2, model 42i-TL for NO_x, model 49i for O_3, model 48i-TLE for CO; Picarro cavity ring-down spectroscopy: Picarro CRDS, G2401 for CO_2 and CH_4; Summa Canister: SILONITE (1869); and GC–MS: Agilent, 7890A/5975C for non-methane hydrocarbon – NMHC), instruments for particulate species detection (time-of-flight aerosol chemical speciation monitor, ToF-ACSM, Aerodyne), and instruments for volatile organic compounds (Vocus proton-transfer reaction time-of-flight mass spectrometer, Vocus-PTR-TOF-MS, Vocus S, Tofwerk, abbreviated as Vocus).

The sampling flow rate of each instrument is calibrated before each experiment. For Thermo Scientific instruments and Vocus, a single standard concentration is tested in each experiment, serving as a basis for instrument status verification and data quantification. For the data collected by ACSM, the calibration is performed based on the mass concentration calculated from SMPS data.

3 Characterization of the AIR chamber

A series of experiments were carried out to evaluate the performance of this chamber system, including leak-proof status, sample-volume support, background concentrations, mixing performance, light characteristics, temperature and RH control, and gas and particle wall loss, as well as characterizations of aerosol particles with the core–shell morphology. All the instruments for measurement are included in Sect. 2.5.

3.1 Fundamental parameters

The leak-proof status of the reactor was characterized by the positive pressure difference between the air inside the reactor and the ambient air and the change in the total number concentration of background particles inside the reactor. When the reactor was filled with zero air, the positive pressure difference inside the reactor was maintained at > 3 Pa within 24 h (Fig. S2a), then it slowly decreased to ∼ 0.5 Pa after several days. When the air inside the reactor was sampled at a flow rate of 5 L min^{-1}, the positive pressure difference decreased to zero after 2 h, and then total particle number concentration slowly increased from ∼ 0 cm^{-3} to a final < 10 cm^{-3} in ∼ 3.5 h (Fig. S2b). This concentration is negligible for a particle number concentration of 10^3–10^4 cm^{-3} that is usually used in experiments. Moreover, this chamber system is designed to operate in batch mode, and the reactor can provide a sampling volume of 1000–1200 L (Fig. S3) and a sampling time of more than 3 h at a total sampling flow rate of 5–6 L min^{-1}. The results above indicate that the system leak-proof status is reliable for further experiments.

The reactor background was also characterized after repeated cleaning with zero air. As shown in Fig. S4, the background particle total number concentration was < 1 cm^{-3} and only increased to 4 cm^{-3} with the mixing fans turned on. Irradiation slightly increased the background particle con-

centration but still only to $< 10\,cm^{-3}$, which is negligible when compared with normal reaction conditions. Table S1 shows the background concentrations of chemical species in the AIR chamber reactor under dry and high RH conditions. Compared with data reported for other chambers (White et al., 2018; Bin Babar et al., 2016; Wang et al., 2014; Platt et al., 2013; Carter et al., 2005; Chen et al., 2019b), the background concentrations of gaseous pollutants including SO_2, NO_x, O_3, and CO in the reactor were comparable or lower for the AIR chamber. The background concentration of total non-methane hydrocarbon (NMHC) was higher than literature values due to the presence of chemically inert $CHClF_2$ (half of the total NMHC concentration), which originates from the indoor refrigeration system and is hard to eliminate within the zero-air generation system. Nevertheless, this species does not interfere with the reactions under most experimental conditions. The reactor can be cleaned to background levels with a volume of zero air > 5 times that of the reactor (Table S2) after each experiment. The cleaning process can be completed in less than 9 h, as shown in Sect. 2.2.

The mixing performance of the injection into the reactor was examined using NO_2 concentration and total particle number concentration as tracers (Fig. S5). The mixing time to uniformity (the duration between the two plateaus in Fig. S5) was 5 min without running fans and less than 1 min with the fans on. Furthermore, the mixing time was independent of the fan speed.

3.2 Light source characterization

The reflective inner wall (SUS304, stainless steel, 8 K, mirror plate) of the AIR chamber is equipped with 40 UV lamps (1.2 m, 40 W, Bulb-T12, GE, USA) to provide irradiation during the experiments. There are 10 lamps on the left, right, back, and top of the wall, respectively, and each lamp can be turned on or off separately by the control system so that the light intensity in experiments varies from 2.5 % to 100 % intensity. These light sources can also be replaced by lamps with different emission spectra to provide a variety of irradiation conditions.

For current light sources, a portable UV spectrometer (StellarNet Inc., Tampa, FL, USA) was used to characterize the irradiance spectrum in the reactor (Fig. S6). The irradiance is mainly distributed in the range of 360–390 nm, peaking at 370 nm, which is within the range of peak irradiance of UV lights used in other indoor chambers (340–371 nm) (Wang et al., 2014; Ma et al., 2022; Bin Babar et al., 2016; Chen et al., 2019b; Lane and Tang, 1994; Thuner et al., 2004). Another small peak appears at 405 nm, which is convenient for directly checking the status of the lamps.

The photolytic rate constant for NO_2 can be used to characterize the irradiation intensity. Previous literature records (Wang et al., 2014; Bin Babar et al., 2016; Ma et al., 2022) often characterize irradiation intensity through the photolytic rate constant of NO_2 (J_{NO_2}), calculated through the steady-state concentrations of NO_x and O_3 (Atkinson et al., 2004). This study mainly used a spectrometer, namely the J-value instrument (AVANTES, AvaSpec-ULS-TEC-EVO) to measure the irradiance and directly calculate the photolytic rate constants of a few important species in atmospheric photochemistry. Notably, the J-value instrument was also calibrated using the J_{NO_2} values derived from the steady NO_x–O_3 concentration under several light schemes to correct for the geometry defect of the J-value instrument when placed inside the AIR chamber. The calibration factor of the traditional J_{NO_2} method is 1.49 ± 0.06. As shown in Table S3, the current light source is more suitable for the photolysis of HONO and NO_2 (photolytic rate constants in the order of 10^{-4}–$10^{-3}\,s^{-1}$). However, the photolysis of HCHO, H_2O_2, and O_3 is slow (photolytic rate constants in the order of 10^{-8}–$10^{-7}\,s^{-1}$). The J_{NO_2} maxima of other chambers are usually in the range of 2–9 $\times\, 10^{-3}\,s^{-1}$ (Chen et al., 2019a; Li et al., 2017; Wang et al., 2014; Bin Babar et al., 2016; Ma et al., 2022). In comparison, J_{NO_2} due to the light source in the AIR chamber is $4.10 \times 10^{-3}\,s^{-1}$, close to the median value of the other chambers. Moreover, the photolytic rate constant of HONO due to the light source in this chamber (J_{HONO} at the level of $10^{-4}\,s^{-1}$) is comparable to or slightly higher than the value of HONO photolysis in the ambient atmosphere in China (J_{HONO} at the level of 10^{-5}–$10^{-4}\,s^{-1}$) (Zheng et al., 2020).

When only lamps on two sides of the AIR chamber were turned on (four schemes with 20 lights on, noted as "only back/top", "left and right", "odd" and "even" in Table S3), the photolytic rate constants in the reactor under different configurations were almost the same ($J_{HONO} = 5.10 \pm 0.12 \times 10^{-4}\,s^{-1}$, $J_{NO_2} = 2.16 \pm 0.05 \times 10^{-3}\,s^{-1}$) and nearly equal to half of that with all 40 lights on. In addition, the photolytic rate constant of the scheme "left and right" (20 lights) was the sum of that of "only left" (10 lights) and "only right" (10 lights). These results indicate that the irradiation in the reactor is uniformly distributed. Notably, because the measurement interface of the J value was a little biased to the left during detection, the value for "only left" was higher than that for "only right".

3.3 Performance of temperature and RH control

The temperature and RH in the reactor are measured by a high-accuracy sensor (HMP110, Vaisala, Finland). Detailed descriptions of temperature and RH control are given in Sect. 2.1 and 2.2. The internal design of our chamber enclosure ensures that the circulating air, which controls the temperature surrounding the reactor, reaches equilibrium (taking < 2 h as shown in Fig. 2) from the outside of the Teflon film to the inside. This design guarantees that the temperature distribution is spatially homogeneous, even for a chamber system with a $30\,m^3$ reactor (Wang et al., 2014). The accuracy for RH of this sensor is shown by its measurement error of < 1 % from that measured by a hygrometer (chilled mirror

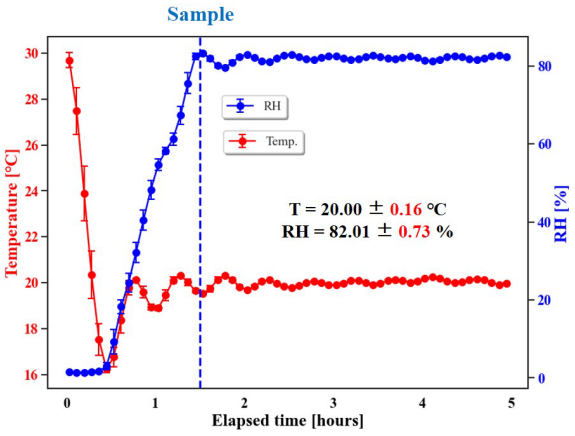

Figure 2. Stability of temperature and RH control in the reactor during sampling. The chamber was operated in batch mode.

hygrometer, Edgetech Instruments, USA) with $R^2 > 0.99$. The temperature in the reactor can be stably controlled in the range of 2.5–31 °C, and the control range of RH is < 2 %–> 95 %. The fluctuations in the temperature inside the reactor are within ±0.15 °C of any set temperature, and the corresponding RH fluctuations for RH > 80 % are within ±0.75 %. The RH fluctuation caused by the water permeation through the FEP filter can be ignored due to the slow permeation rate of water molecules ($0.007\,\mathrm{L\,m^{-2}\,(24\,h)^{-1}\,atm^{-1}}$). The stability achieved with the temperature and RH controls across a wide range of temperatures is shown in Table S4. The illumination of lamps raises the lowest achievable temperature by 3 °C for every 10 lights on. However, the illumination of the reactor does not affect the stability of temperature and RH inside the reactor. When the set temperature is close to room temperature (20 °C in Table S4), the fluctuation is < 0.1 °C, demonstrating a more accurate temperature and RH control performance compared with other chambers (Table S5) (Wang et al., 2014; Wu et al., 2007; Bin Babar et al., 2016; Ma et al., 2022; W. G. Wang et al., 2015). Sampling operation (lasting more than 3 h with flow rate at $5\,\mathrm{L\,min^{-1}}$, Fig. 2) does not significantly affect the stability of temperature and RH control either, which also indicates that the permeation and wall loss of water molecules do not affect a lot.

In order to simulate the diurnal variations in ambient air temperature and RH, a proportional–integral–derivative (PID) feedback controlling function was designed. The RH in the reactor can reach the target RH by controlling the temperature. After receiving the target RH input, the control programme calculates the stepwise theoretical RH value at each time increment and the corresponding temperature control steps based on current temperature and RH in the reactor. This calculation is also adjusted in real time to optimize the gradual change of RH. Figure S7 demonstrates two examples to show alternate linear change and constant control of RH. The RH can reach the set value within a few hours with fluctuations < 0.75 %. This function performs even better at low temperatures, suggesting the potential of using this chamber system to simulate diurnal variations of RH in the ambient atmosphere in wintertime.

3.4 Wall loss of gas and particles

The wall loss process is considered as a first-order kinetic process in that the decay rate of a concentration is proportional to the concentration:

$$\frac{\mathrm{d}C(t)}{\mathrm{d}t} = -k \cdot C(t), \tag{1}$$

where $C(t)$ is the species concentration at time t, and k is the wall loss rate constant (in units $\mathrm{min^{-1}}$). The wall loss rates of gaseous species such as NO_x and O_3 in this study are shown in Table S6, the values of which are lower than other small Teflon chambers (2–5 $\mathrm{m^3}$) (Wu et al., 2007; W. G. Wang et al., 2015; Li et al., 2017; Bernard et al., 2016) as a result of passivation of the inner surface of the reactor with 2 ppm O_3 for 3 d. In Table S6, when the fans are turned on, the wall loss is usually much higher; therefore, the fans will only be turned on during the injection period, and when simulating the reaction and sampling, the fans are kept off.

The wall loss rate constant k of particles is dependent on particle size (diameter, noted as D_p). Smaller or larger particles often have higher k values (Crump and Seinfeld, 1981) due to higher diffusion or sedimentation rates, respectively. The dependence of k values for particles with $D_\mathrm{p} < 50$ nm is rarely reported in previous chamber studies. This study demonstrates that the constant k decreases as a function of decreasing D_p when particles are smaller than 50 nm, which is also shown in Fig. S7 of Ma et al. (2022). The $\log_{10}(k)$ value for particles can be approximated with a segmented linear function of $\log_{10}(D_\mathrm{p})$[93,94]. In addition to the slopes to be determined, the inflection point D_p, where the loss trend inverses, changes with different chambers. In this study, two inflection points are selected at 50 and 150 nm according to the identified inflection particle size bin of 45.3–53.2 and 143.3–165.5 nm, respectively (Fig. S8). Furthermore, the k–D_p dependence has been reported to deviate in different experiments, even in the same reactor. This study found that such deviations can be corrected through an up-and-down shift of the $\log_{10}(k) - \log_{10}(D_\mathrm{p})$ function curve. Even for deliquescent particles (RH = 90 % in Fig. S8, the D_p of the x axis represents the liquid particle diameters), this method still accurately described the relationship between k and D_p ($R^2 \sim 0.95$) when considering the hygroscopic growth of the particle size.

Another commonly used parameter to characterize the particle wall loss behaviour in chambers is the total volume wall loss rate constant (k_v). For small Teflon chambers of 2–3 $\mathrm{m^3}$ in size (Takekawa et al., 2003; Li et al., 2017; Liu et al., 2019), k_v values typically range from 2.84–$4.72 \times 10^{-3}\,\mathrm{min^{-1}}$. The particle wall loss is slightly higher

in the chamber in this study, with the k_v found to be 5×10^{-3} min^{-1} (Table S7).

3.5 Morphology of seed particle generation

Seed particles are typically used to simulate aerosol formation by the multiphase chemistry pathway. The AIR chamber is designed to be coupled to a subsystem for generating seed particles with different phase states through predeliquescing, adopted from a previous study (Faust et al., 2017). A volatilizing–condensing method is used to generate known-composition organic-coated inorganic particles in the AIR chamber, with a detailed description in Sect. 2.4.

As shown in Fig. 3, squalane is coated onto dry 200 nm monodisperse NaCl seed particles to produce a core–shell morphology for the particles. The coating thickness is controlled by adjusting the water bath heating temperature while maintaining a fixed condensation temperature of 20 °C. The surface area concentrations of the introduced seed ($> 800\,\mu m^2\,cm^{-3}$) are sufficient that no homogeneous nucleation of organic vapour occurs. Both the size distributions of the particles before and after condensing organics on the particles are monodisperse. Using the Clausius–Clapeyron equation that describes the relationship between saturation vapour pressure and temperature, as well as the Maxwell equation that describes the condensation growth rate of particle size under a certain supersaturated vapour pressure, the coating thickness can be predicted in relation to the heating temperature (Fig. 3a) to assess the feasibility of the selected coating species. The coating thickness is calculated as half of the difference in peak D_p of the monodisperse particle size distribution before and after the seeds are coated (Fig. 3b). For squalane, the device allows for a relatively accurate control of coating thickness in the range of 5 to 25 nm (1 %–12 % shell thickness). For organic species with similar volatilities (saturated vapour pressure in the order of 10^{-4}–10^{-5} mm Hg at room temperature), the device could provide similar control performance.

4 Applications in SOA generation – α-pinene ozonolysis research

4.1 SOA yield of seed-absent experiments

SOAs are generated from α-pinene ozonolysis in the AIR chamber to evaluate its performance, with experiment conditions given in Table S8 (Nos. 1–5). The key parameter Y, representing the yield of SOAs, is defined as:

$$Y = \frac{\Delta mo}{\Delta ROG}, \quad (2)$$

where Δmo represents the total mass concentration of generated SOAs, and ΔROG represents the total mass concentration of reactive organic gas that was consumed in the reaction (specifically referring to α-pinene in this study), with both units in micrograms per cubic metre ($\mu g\,m^{-3}$). The SOA mass concentration was measured by a ToF-ACSM (Sect. 2.5). The organic mass measurement was also corrected based on the particle size distribution data from SMPS, where the α-pinene-derived SOA density was assumed as $1.3\,g\,cm^{-3}$. This density value is also used in much previous research (Bahreini et al., 2005; Alfarra et al., 2006; Ma et al., 2022), but it is higher than the unit density assumption used in some other chamber studies (Wang et al., 2011, 2014; Bin Babar et al., 2016; Cocker et al., 2001b; Li et al., 2021; Zhang et al., 2015).

Odum et al. (1996) found that the non-linear relationship between the SOA yield Y and the particulate organic mass concentration (mo) is well reproduced by the two-product model:

$$Y = mo \cdot \sum \frac{\alpha_i \cdot K_{om,i}}{1 + mo \cdot K_{om,i}}, \quad (3)$$

where α_i and $K_{om,i}$ are the mass-based stoichiometric and partition coefficient for species i, respectively, and mo is the total mass concentration of organic aerosol. Figure 4 shows the results of the two-product model that fits the seed-absent SOA yield results in this study. The Odum model fit results from other chamber studies are also shown in Fig. 4 for comparison. Detailed model fitting parameters are shown in Table S9. In contrast, Y in this study is a little higher than those in other small- or medium-sized chambers, which may be due to the lower gas wall loss in our Teflon reactor (Sect. 3.4) and the lower experimental temperature. The four fitting parameters in this study – α_1, α_2, K_1, and K_2 – are 0.62479, 0.0326791, 0.0121589, and 0.0121596, respectively; K_1 and K_2 are close and moderate values. However, α_1 is significantly higher than those in other chambers. Such higher values for α_1 can be an indication of a lower volatilizing loss of the gas phase intermediates within the AIR reactor compared with the other chambers. The good fitting from our experiment indicates that the chamber system in this study is stable. These results imply a reliable performance of our chamber system for experimental simulation studies of atmospheric secondary transformation process.

4.2 Effects of seed phase state on SOA yield

The effects of different seed phase states on the yield of α-pinene-derived SOA were further investigated using ammonium sulfate as the seed particles (Table S8, Nos. 6–8). We used seeds with sufficient surface area concentration to prevent the gas phase products of VOCs from homogeneous nucleation. Figure S11 shows the relevant measured parameters during one reaction (e.g. experiment No. 8). The yields of all the experiments are summarized in Fig. 5. In general, the yield in the presence of dry seeds is not significantly different from that in the absence of seeds, consistent with the outcome of Odum et al. (1996). However, in the presence of aerosol liquid water and ammonium sulfate seeds,

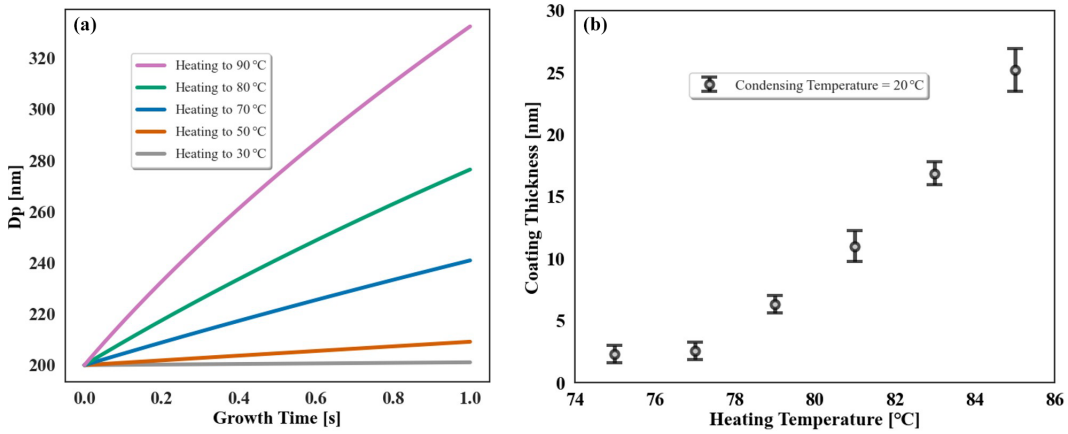

Figure 3. Relationship between coating thickness on dry 200 nm NaCl seed and heating temperature in the coating device, with squalane as the coating species and condensation temperature of 20 °C. **(a)** Theoretical estimation in different growth times. **(b)** Measured results by SMPS.

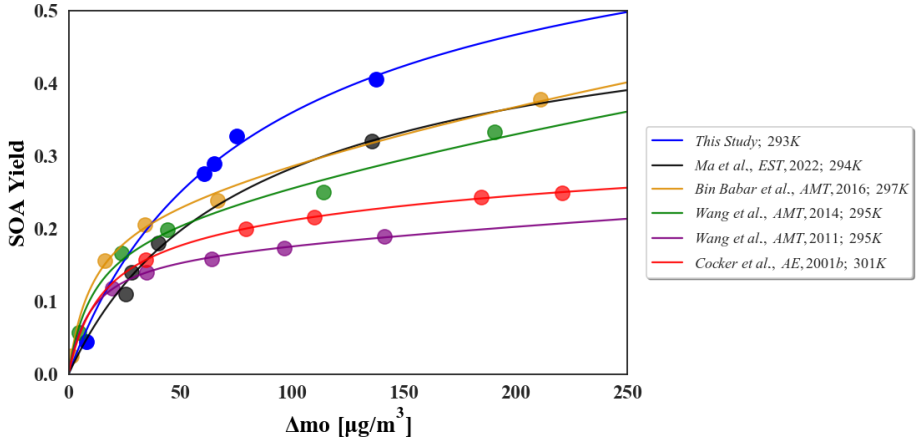

Figure 4. Two-product model fitting curve of seed-absent α-pinene-derived SOA yield in this study and the comparison with other literature results. The data of the blue line are from this study, and other data are obtained from these references: Cocker et al., 2001b; Wang et al., 2011, 2014; Bin Babar et al., 2016; Ma et al., 2022.

the α-pinene-derived SOA yield is reduced. This suppressing phenomenon is also reported by Cocker et al. (2001b), which may be related to the finding of Lutz et al. (2019) that the presence of high sulfate levels may inhibit the partitioning of organic species into the particulate phase. However, to our knowledge, the suppressing phenomenon above may not be common since it has only been reported in the α-pinene ozonolysis system with ammonium sulfate seeds.

The subplot in Fig. 5 demonstrates the SOA yield at each elapsed time point in these experiments. Liquid water can significantly promote the initial SOA yield and generation rate (Zhang et al., 2018), and our results have reproduced this phenomenon (subplot in Fig. 5). However the oxidation reaction proceeds, it is observed that the SOA yield with liquid seeds decreases and larger seed aerosol liquid water contents produce greater decreases in the yield. These indicate that the AIR chamber system facilitates research on aerosol properties in atmospheric multiphase processes.

It is worth noting that the organic vapour wall loss can have significant influence on SOA formation. However, quantifying wall losses of gaseous organic products is still a challenge in chamber experiments. Gaseous intermediates are difficult to be quantitatively measured, and the theoretical calculations of wall losses also have large uncertainties due to the lack of data on some parameters, such as the effective wall mass concentration and eddy diffusion coefficient inside the reactor. The wall loss behaviour of gases essentially depends on the concentration gradient between the gas phase and the wall. To our knowledge, there is no conclusive evidence to support higher wall losses of gaseous intermediates under higher RH, which are even significant enough to cause a notable reduction in SOA yield. In addition, if higher RH can enhance the diffusion of gaseous intermedi-

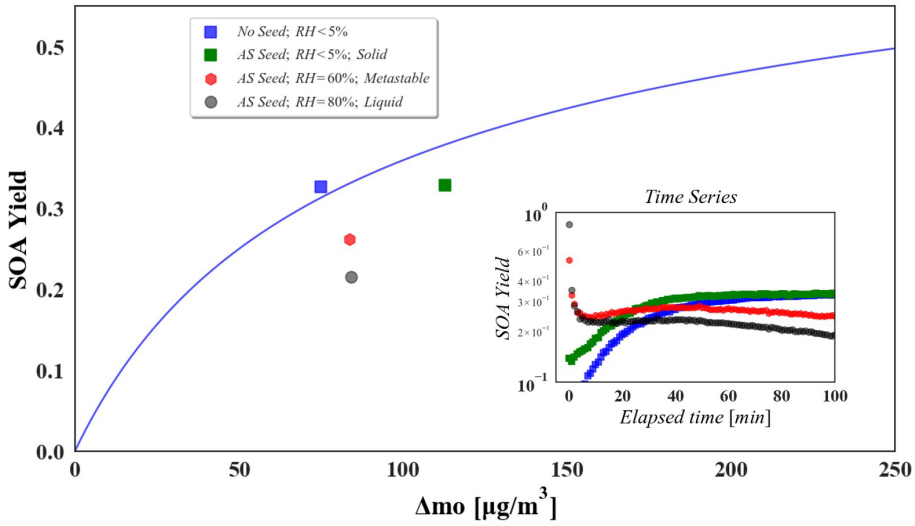

Figure 5. Effects of phase state and liquid water content of ammonium sulfate seed particles on the SOA yield of α-pinene ozonolysis (α-pinene $= 60 \pm 13$ ppb, $O_3 = 296 \pm 30$ ppb). In the main plot, the blue line is the fitting two-product curve from the no-seed experiment data in this study, which is a replicate of the curve in Fig. 4. The subplot shows the current yield since the initial time point of each experiment, where the blue points represent the data of the no-seed experiment, green points represent the data of the solid seed experiment, red points represent the data of the metastable seed experiment, and grey points represent the data of the liquid seed experiment.

ates towards the wall, then the diffusion of gaseous intermediates towards the particle phase should also increase. Compared with experiments without seed particles, when seed particles exist, gases condense on the particles while condensing on the walls, causing the gas–phase concentration to decay more rapidly, resulting in less wall loss of gases and higher SOA yields during the initial period of the experiment, as shown in the subplot of Fig. 5. However, the final difference in SOA yields is still unclear because, under the condition without seed particles, particles generated through nucleation continue to grow and can provide a considerable amount of condensation sink after the reaction proceeds for a period of time. This process needs to be numerically described and analysed to carefully consider wall loss behaviour and physicochemical properties of particles in future studies.

5 Conclusions

The reported special phenomena relying on specific particle properties are well reproduced in AIR chamber benefitting from the seed phase state control, and the accurate temperature and RH control facilitate the quantization of the effects of aerosol liquid water. Besides, compared to other chambers, the manipulation of composition and thickness of organic coating could provide a clearer surface property. Broad temperature range, adjustable irradiation intensity, and the fast-responding RH cycle make this chamber system suitable for simulating diurnal ambient atmosphere in different seasons. These performances of handling key parameters highlight the potential of this AIR chamber system for the laboratory simulation of atmospheric multiphase processes.

Data availability. The data in this study are available from the authors upon request (zhijunwu@pku.edu.cn).

Supplement. The supplement related to this article is available online at: https://doi.org/10.5194/amt-16-3679-2023-supplement.

Author contributions. TZ and ZW conceived the study. TZ, ZW, JW, and WF conducted the laboratory measurements. TZ carried out the data analysis. TZ, KB, YY, XY, ZB, XM, and YZ participated in the instrument managements. SG, YC, CL, YZ, SML, and MH supported this research. TZ wrote the paper with inputs from all co-authors.

Competing interests. The contact author has declared that none of the authors has any competing interests.

Disclaimer. Publisher's note: Copernicus Publications remains neutral with regard to jurisdictional claims in published maps and institutional affiliations.

Acknowledgements. We thank the Beijing Convenient Environmental Tech Co. Ltd. for constructing the chamber.

Financial support. This research has been supported by the National Natural Science Foundation of China (grant nos. 22221004 and 41875149).

Review statement. This paper was edited by Pierre Herckes and reviewed by three anonymous referees.

References

Abbatt, J. P., Lee, A. K., and Thornton, J. A.: Quantifying trace gas uptake to tropospheric aerosol: recent advances and remaining challenges, Chem. Soc. Rev., 41, 6555–6581, https://doi.org/10.1039/c2cs35052a, 2012.

Akimoto, H., Hoshino, M., Inoue, G., Sakamaki, F., Washida, N., and Okuda, M.: Design and characterization of the evacuable and bakable photochemical smog chamber, Environ. Sci. technol, 13, 471–475, 1979.

Albu, M., Barnes, I., and Mocanu, R.: Kinetic Study of the Temperature Dependence of the OH Initiated Oxidation of Dimethyl Sulphide, Springer, Dordrecht, 223–230, https://doi.org/10.1007/1-4020-4232-9_19, 2006.

Alfarra, M. R., Paulsen, D., Gysel, M., Garforth, A. A., Dommen, J., Prévôt, A. S. H., Worsnop, D. R., Baltensperger, U., and Coe, H.: A mass spectrometric study of secondary organic aerosols formed from the photooxidation of anthropogenic and biogenic precursors in a reaction chamber, Atmos. Chem. Phys., 6, 5279–5293, https://doi.org/10.5194/acp-6-5279-2006, 2006.

Atkinson, R., Baulch, D. L., Cox, R. A., Crowley, J. N., Hampson, R. F., Hynes, R. G., Jenkin, M. E., Rossi, M. J., and Troe, J.: Evaluated kinetic and photochemical data for atmospheric chemistry: Volume I – gas phase reactions of O_x, HO_x, NO_x and SO_x species, Atmos. Chem. Phys., 4, 1461–1738, https://doi.org/10.5194/acp-4-1461-2004, 2004.

Bahreini, R., Keywood, M. D., Ng, N. L., Varutbangkul, V., Gao, S., Flagan, R. C., Seinfeld, J. H., Worsnop, D. R., and Jimenez, J. L.: Measurements of secondary organic aerosol from oxidation of cycloalkenes, terpenes, and m-xylene using an Aerodyne aerosol mass spectrometer, Environ. Sci. Technol., 39, 5674–5688, 2005.

Barnes, I.: Kinetics, Products and Mechanism of O(3P) Atom Reactions with Alkyl Iodides, Environmental Simulation Chambers: Application to Atmospheric Chemical Processes, Springer, Dordrecht, 193–205, https://doi.org/10.1007/1-4020-4232-9_16, 2006.

Batchvarova, E., Spassova, T., Valkov, N., and Iordanova, L.: Survey on Atmospheric Chemistry Research in Some New EU Member States and Candidate Countries, Springer, Dordrecht, 301–340, https://doi.org/10.1007/1-4020-4232-9_27, 2006.

Bejan, I., Barnes, I., Olariu, R., Becker, K. H., and Mocanu, R.: FT-IR Kinetic Study on the Gas-Phase Reactions of the OH Radical with a Series of Nitroaromatic Compounds, Springer, Dordrecht, 155–162, https://doi.org/10.1007/1-4020-4232-9_12, 2006.

Berkemeier, T., Steimer, S. S., Krieger, U. K., Peter, T., Pöschl, U., Ammann, M., and Shiraiwa, M.: Ozone uptake on glassy, semi-solid and liquid organic matter and the role of reactive oxygen intermediates in atmospheric aerosol chemistry, Phys. Chem. Chem. Phys., 18, 12662–12674, https://doi.org/10.1039/c6cp00634e, 2016.

Bernard, F., Ciuraru, R., Boreave, A., and George, C.: Photosensitized Formation of Secondary Organic Aerosols above the Air/Water Interface, Environ. Sci. Technol., 50, 8678–8686, 2016.

Bin Babar, Z., Park, J. H., Kang, J., and Lim, H. J.: Characterization of a Smog Chamber for Studying Formation and Physicochemical Properties of Secondary Organic Aerosol, Aerosol Air Qual. Res., 16, 3102–3113, 2016.

Bohn, B., Rohrer, F., Brauers, T., and Wahner, A.: Actinometric measurements of NO_2 photolysis frequencies in the atmosphere simulation chamber SAPHIR, Atmos. Chem. Phys., 5, 493–503, https://doi.org/10.5194/acp-5-493-2005, 2005.

Brauers, T., Bohn, B., Johnen, F.-J., Rohrer, R., Rodriguez Bares, S., Tillmann, R., and Wahner, A.: The atmosphere simulation chamber SAPHIR: a tool for the investigation of photochemistry, EGS - AGU - EUG Joint Assembly, Nice, France, 6–11 April 2003, abstract id. 4449, https://ui.adsabs.harvard.edu/abs/2003EAEJA.....4449B (last access: 25 July 2023), 2003.

Brunamonti, S., Krieger, U. K., Marcolli, C., and Peter, T.: Redistribution of black carbon in aerosol particles undergoing liquid-liquid phase separation, Geophys. Res. Lett., 42, 2532–2539, 2015.

Carter, W. P. L.: Environmental Chamber Studies of Ozone Formation Potentials of Volatile Organic Compounds, Springer, Dordrecht, 231–240, https://doi.org/10.1007/1-4020-4232-9_20, 2006.

Carter, W. P. L. and Lurmann, F. W.: Evaluation Of a Detailed Gas-Phase Atmospheric Reaction-Mechanism Using Environmental Chamber Data, Atmos. Environ. A-Gen., 25, 2771–2806, 1991.

Carter, W. P. L., Atkinson, R., Winer, A. M., and Pitts, J. N.: Experimental Investigation Of Chamber-Dependent Radical Sources, Int. J. Chem. Kinet., 14, 1071–1103, 1982.

Carter, W. P. L., Cocker, D. R., Fitz, D. R., Malkina, I. L., Bumiller, K., Sauer, C. G., Pisano, J. T., Bufalino, C., and Song, C.: A new environmental chamber for evaluation of gas-phase chemical mechanisms and secondary aerosol formation, Atmos. Environ.ment, 39, 7768–7788, 2005.

Chen, B. B. and Lelevkin, V. M.: Influence of Atmospheric Aerosol Contamination on the Regional Climate in Central Asia, Springer, Dordrecht, 403–414, https://doi.org/10.1007/1-4020-4232-9_34, 2006.

Chen, T. Z., Liu, Y. C., Liu, C. G., Liu, J., Chu, B. W., and He, H.: Important role of aromatic hydrocarbons in SOA formation from unburned gasoline vapor, Atmos. Environ., 201, 101–109, 2019a.

Chen, T., Liu, Y., Ma, Q., Chu, B., Zhang, P., Liu, C., Liu, J., and He, H.: Significant source of secondary aerosol: formation from gasoline evaporative emissions in the presence of SO_2 and NH_3, Atmos. Chem. Phys., 19, 8063–8081, https://doi.org/10.5194/acp-19-8063-2019, 2019b.

Cheng, Y., Su, H., Koop, T., Mikhailov, E., and Poschl, U.: Size dependence of phase transitions in aerosol nanoparticles, Nat. Commun., 6, 5923, https://doi.org/10.1038/ncomms6923, 2015.

Cocker, D. R., Flagan, R. C., and Seinfeld, J. H.: State-of-the-art chamber facility for studying atmospheric aerosol chemistry, Environ. Sci. Technol., 35, 2594–2601, 2001a.

Cocker III, D. R., Clegg, S. L., Flagan, R. C., and Seinfeld, J. H.: The effect of water on gas–particle partitioning of secondary organic aerosol. Part I: α-pinene/ozone system, Atmos. Environ.,

35, 6049–6072, https://doi.org/10.1016/S1352-2310(01)00404-6, 2001b.

Corral Arroyo, P., Bartels-Rausch, T., Alpert, P. A., Dumas, S., Perrier, S., George, C., and Ammann, M.: Particle-Phase Photosensitized Radical Production and Aerosol Aging, Environ. Sci. Technol., 52, 7680–7688, https://doi.org/10.1021/acs.est.8b00329, 2018.

Cosman, L. M. and Bertram, A.: Reactive Uptake of N_2O_5 on Aqueous H_2SO_4 Solutions Coated with 1-Component and 2-Component Monolayers, J. Phys. Chem. A, 112, 4625–4635, https://doi.org/10.1021/jp8005469, 2008.

Crump, J. G. and Seinfeld, J. H.: Turbulent Deposition And Gravitational Sedimentation Of an Aerosol In a Vessel Of Arbitrary Shape, J. Aerosol Sci., 12, 405–415, 1981.

Davidovits, P., Kolb, C. E., Williams, L. R., Jayne, J. T., and Worsnop, D. R.: Update 1 of: Mass Accommodation and Chemical Reactions at Gas-Liquid Interfaces, Chem. Rev., 111, PR76–109, https://doi.org/10.1021/cr100360b, 2011.

Dodge, M. C.: Chemical oxidant mechanisms for air quality modeling: critical review, Atmos. Environ., 34, 2103–2130, 2000.

Faust, J. A., Wong, J. P., Lee, A. K., and Abbatt, J. P.: Role of Aerosol Liquid Water in Secondary Organic Aerosol Formation from Volatile Organic Compounds, Environ. Sci. Technol., 51, 1405–1413, https://doi.org/10.1021/acs.est.6b04700, 2017.

Fleming, L. T., Lin, P., Roberts, J. M., Selimovic, V., Yokelson, R., Laskin, J., Laskin, A., and Nizkorodov, S. A.: Molecular composition and photochemical lifetimes of brown carbon chromophores in biomass burning organic aerosol, Atmos. Chem. Phys., 20, 1105–1129, https://doi.org/10.5194/acp-20-1105-2020, 2020.

Franco, B., Blumenstock, T., Cho, C., Clarisse, L., Clerbaux, C., Coheur, P. F., De Maziere, M., De Smedt, I., Dorn, H. P., Emmerichs, T., Fuchs, H., Gkatzelis, G., Griffith, D. W. T., Gromov, S., Hannigan, J. W., Hase, F., Hohaus, T., Jones, N., Kerkweg, A., Kiendler-Scharr, A., Lutsch, E., Mahieu, E., Novelli, A., Ortega, I., Paton-Walsh, C., Pommier, M., Pozzer, A., Reimer, D., Rosanka, S., Sander, R., Schneider, M., Strong, K., Tillmann, R., Van Roozendael, M., Vereecken, L., Vigouroux, C., Wahner, A., and Taraborrelli, D.: Ubiquitous atmospheric production of organic acids mediated by cloud droplets, Nature, 593, 233–237, https://doi.org/10.1038/s41586-021-03462-x, 2021.

George, C., Ammann, M., D'Anna, B., Donaldson, D. J., and Nizkorodov, S. A.: Heterogeneous photochemistry in the atmosphere, Chem. Rev., 115, 4218–4258, https://doi.org/10.1021/cr500648z, 2015.

George, I. J. and Abbatt, J. P.: Heterogeneous oxidation of atmospheric aerosol particles by gas-phase radicals, Nat. Chem., 2, 713–722, https://doi.org/10.1038/nchem.806, 2010.

Griffin, R. J., Cocker, D. R., Flagan, R. C., and Seinfeld, J. H.: Organic aerosol formation from the oxidation of biogenic hydrocarbons, J. Geophys. Res.-Atmos., 104, 3555–3567, 1999.

Haagensmit, A. J.: Chemistry And Physiology Of Los-Angeles Smog, Ind. Eng. Chem., 44, 1342–1346, 1952.

Hallquist, M., Wenger, J. C., Baltensperger, U., Rudich, Y., Simpson, D., Claeys, M., Dommen, J., Donahue, N. M., George, C., Goldstein, A. H., Hamilton, J. F., Herrmann, H., Hoffmann, T., Iinuma, Y., Jang, M., Jenkin, M. E., Jimenez, J. L., Kiendler-Scharr, A., Maenhaut, W., McFiggans, G., Mentel, Th. F., Monod, A., Prévôt, A. S. H., Seinfeld, J. H., Surratt, J. D., Szmigielski, R., and Wildt, J.: The formation, properties and impact of secondary organic aerosol: current and emerging issues, Atmos. Chem. Phys., 9, 5155–5236, https://doi.org/10.5194/acp-9-5155-2009, 2009.

Herrmann, H., Schaefer, T., Tilgner, A., Styler, S. A., Weller, C., Teich, M., and Otto, T.: Tropospheric aqueous-phase chemistry: kinetics, mechanisms, and its coupling to a changing gas phase, Chem. Rev., 115, 4259–4334, https://doi.org/10.1021/cr500447k, 2015.

Hidy, G. M.: Atmospheric Chemistry in a Box or a Bag, Atmosphere-Basel, 10, 401, https://doi.org/10.3390/atmos10070401, 2019.

Hu, C. J., Cheng, Y., Pan, G., Gai, Y. B., Gu, X. J., Zhao, W. X., Wang, Z. Y., Zhang, W. J., Chen, J., Liu, F. Y., Shan, X. B., and Sheng, L. S.: A Smog Chamber Facility for Qualitative and Quantitative Study on Atmospheric Chemistry and Secondary Organic Aerosol, Chin. J. Chem. Phys., 27, 631–639, 2014.

Hurley, M. D., Sokolov, O., Wallington, T. J., Takekawa, H., Karasawa, M., Klotz, B., Barnes, I., and Becker, K. H.: Organic aerosol formation during the atmospheric degradation of toluene, Environ. Sci. Technol., 35, 1358–1366, 2001.

Johnson, D., Jenkin, M. E., Wirtz, K., and Martin-Reviejo, M.: Simulating the Formation of Secondary Organic Aerosol from the Photooxidation of Toluene, Environ. Chem., 1, 150–165, 2004.

Kang, E., Root, M. J., Toohey, D. W., and Brune, W. H.: Introducing the concept of Potential Aerosol Mass (PAM), Atmos. Chem. Phys., 7, 5727–5744, https://doi.org/10.5194/acp-7-5727-2007, 2007.

Kolev, S., Grigorieva, V.: Surface and Total Ozone Over Bulgaria, in: Environmental Simulation Chambers: Application to Atmospheric Chemical Processes, edited by: Barnes, I. and Rudzinski, K. J., Nato Science Series: IV: Earth and Environmental Science, Vol. 62, Springer, Dordrecht, https://doi.org/10.1007/1-4020-4232-9_29, 2006.

Lambe, A. T., Chhabra, P. S., Onasch, T. B., Brune, W. H., Hunter, J. F., Kroll, J. H., Cummings, M. J., Brogan, J. F., Parmar, Y., Worsnop, D. R., Kolb, C. E., and Davidovits, P.: Effect of oxidant concentration, exposure time, and seed particles on secondary organic aerosol chemical composition and yield, Atmos. Chem. Phys., 15, 3063–3075, https://doi.org/10.5194/acp-15-3063-2015, 2015.

Lane, D. A. and Tang, H.: Photochemical Degradation of Polycyclic Aromatic Compounds. I. Naphthalene, Polycycl. Aromat. Comp., 5, 131–138, 1994.

Leone, J. A., Flagan, R. C., Grosjean, D., and Seinfeld, J. H.: An Outdoor Smog Chamber And Modeling Study Of Toluene-NO_x Photooxidation, Int. J. Chem. Kinet., 17, 177–216, 1985.

Leone, J. A., Flagan, R. C., Grosjean, D., and Seinfeld, J. H.: An outdoor smog chamber and modeling study of toluene–NO_x photooxidation, Int. J. Chem. Kinet., 17, 177–216, 2010.

Li, J. L., Li, H., Wang, X. Z., Wang, W. G., Ge, M. F., Zhang, H., Zhang, X., Li, K., Chen, Y., Wu, Z. H., Chai, F. H., Meng, F., Mu, Y. J., Mellouki, A., Bi, F., Zhang, Y. J., Wu, L. Y., and Liu, Y. C.: A large-scale outdoor atmospheric simulation smog chamber for studying atmospheric photochemical processes: Characterization and preliminary application, J. Environ. Sci.-China, 102, 185–197, 2021.

Li, K. W., Chen, L. H., Han, K., Lv, B. A., Bao, K. J., Wu, X. C., Gao, X., and Cen, K. F.: Smog chamber study on aging

of combustion soot in isoprene/SO_2/NO_x system: Changes of mass, size, effective density, morphology and mixing state, Atmos. Res., 184, 139–148, 2017.

Liu, S. J., Tsona, N. T., Zhang, Q., Jia, L., Xu, Y. F., and Du, L.: Influence of relative humidity on cyclohexene SOA formation from OH photooxidation, Chemosphere, 231, 478–486, 2019.

Liu, T., Chan, A. W. H., and Abbatt, J. P. D.: Multiphase Oxidation of Sulfur Dioxide in Aerosol Particles: Implications for Sulfate Formation in Polluted Environments, Environ. Sci. Technol., 55, 4227–4242, https://doi.org/10.1021/acs.est.0c06496, 2021.

Liu, T. Y. and Abbatt, J. P. D.: Oxidation of sulfur dioxide by nitrogen dioxide accelerated at the interface of deliquesced aerosol particles, Nat. Chem., 13, 1173–1177, https://doi.org/10.1038/s41557-021-00777-0, 2021.

Lutz, A., Mohr, C., Le Breton, M., Lopez-Hilfiker, F. D., Priestley, M., Thornton, J. A., and Hallquist, M.: Gas to Particle Partitioning of Organic Acids in the Boreal Atmosphere, ACS Earth Space Chem., 3, 1279–1287, https://doi.org/10.1021/acsearthspacechem.9b00041, 2019.

Ma, W., Liu, Y., Zhang, Y., Feng, Z., Zhan, J., Hua, C., Ma, L., Guo, Y., Zhang, Y., Zhou, W., Yan, C., Chu, B., Chen, T., Ma, Q., Liu, C., Kulmala, M., Mu, Y., and He, H.: A New Type of Quartz Smog Chamber: Design and Characterization, Environ. Sci. Technol., 56, 2181–2190, https://doi.org/10.1021/acs.est.1c06341, 2022.

Martin-Reviejo, M. and Wirtz, K.: Is benzene a precursor for secondary organic aerosol?, Environ. Sci. Technol., 39, 1045–1054, 2005.

Mekic, M., Liu, J., Zhou, W., Loisel, G., and Gligorovski, S.: Formation of highly oxygenated multifunctional compounds from cross-reactions of carbonyl compounds in the atmospheric aqueous phase, Atmos. Environ., 219, 117046, https://doi.org/10.1016/j.atmosenv.2019.117046, 2019.

Mellouki, A.: Atmospheric Fate of Unsaturated Ethers, Springer, Dordrecht, 163–169, https://doi.org/10.1007/1-4020-4232-9_13, 2006.

Mocanu, R., Cucu-Man, S., and Steinnes, E.: Heavy Metals Pollution: An Everlasting Problem, Springer, Dordrecht, 359–368, https://doi.org/10.1007/1-4020-4232-9_30, 2006.

Morriss, F. V., Bolze, C., Goodwin, J. T., and King, F.: Smog Experiments In Large Chambers, Ind. Eng. Chem., 49, 1249–1250, 1957.

Odum, J. R., Hoffmann, T., Bowman, F., Collins, D., Flagan, R. C., and Seinfeld, J. H.: Gas/particle partitioning and secondary organic aerosol yields, Environ. Sci. Technol., 30, 2580–2585, 1996.

Odum, J. R., Jungkamp, T. P. W., Griffin, R. J., Forstner, H. J. L., Flagan, R. C., and Seinfeld, J. H.: Aromatics, reformulated gasoline, and atmospheric organic aerosol formation, Environ. Sci. Technol., 31, 1890–1897, 1997.

Olariu, R.-I., Duncianu, M., Arsene, C., and Wirtz, K.: Determination of Photolysis Frequencies for Selected Carbonyl Compounds in the EUPHORE Chamber Environmental, Springer, Dordrecht, 121–128, https://doi.org/10.1007/1-4020-4232-9_9, 2006.

Pandis, S. N., Paulson, S. E., Seinfeld, J. H., and Flagan, R. C.: Aerosol Formation In the Photooxidation Of Isoprene And Beta-Pinene, Atmos. Environ. A-Gen, 25, 997–1008, 1991.

Paulsen, D., Dommen, J., Kalberer, M., Prévôt, A. S. H., Richter, R., Sax, M., Steinbacher, M., Weingartner, E., and Baltensperger, U.: Secondary organic aerosol formation by irradiation of 1,3,5-trimethylbenzene-NO_x-H_2O in a new reaction chamber for atmospheric chemistry and physics, Environ. Sci. Technol., 39, 2668–2678, https://doi.org/10.1021/es0489137, 2005.

Peng, J., Hu, M., Guo, S., Du, Z., Shang, D., Zheng, J., Zheng, J., Zeng, L., Shao, M., Wu, Y., Collins, D., and Zhang, R.: Ageing and hygroscopicity variation of black carbon particles in Beijing measured by a quasi-atmospheric aerosol evolution study (QUALITY) chamber, Atmos. Chem. Phys., 17, 10333–10348, https://doi.org/10.5194/acp-17-10333-2017, 2017.

Platt, S. M., El Haddad, I., Zardini, A. A., Clairotte, M., Astorga, C., Wolf, R., Slowik, J. G., Temime-Roussel, B., Marchand, N., Ježek, I., Drinovec, L., Močnik, G., Möhler, O., Richter, R., Barmet, P., Bianchi, F., Baltensperger, U., and Prévôt, A. S. H.: Secondary organic aerosol formation from gasoline vehicle emissions in a new mobile environmental reaction chamber, Atmos. Chem. Phys., 13, 9141–9158, https://doi.org/10.5194/acp-13-9141-2013, 2013.

Pöschl, U. and Shiraiwa, M.: Multiphase chemistry at the atmosphere-biosphere interface influencing climate and public health in the anthropocene, Chem. Rev., 115, 4440–4475, https://doi.org/10.1021/cr500487s, 2015.

Pratap, V., Carlton, A. G., Christiansen, A. E., and Hennigan, C. J.: Partitioning of Ambient Organic Gases to Inorganic Salt Solutions: Influence of Salt Identity, Ionic Strength, and pH, Geophys. Res. Lett., 48, e2021GL095247, https://doi.org/10.1029/2021gl095247, 2021.

Ravishankara, A. R.: Heterogeneous and multiphase chemistry in the troposphere, Science, 276, 1058–1065, 1997.

Reid, J. P., Bertram, A. K., Topping, D. O., Laskin, A., Martin, S. T., Petters, M. D., Pope, F. D., and Rovelli, G.: The viscosity of atmospherically relevant organic particles, Nat. Commun., 9, 956, https://doi.org/10.1038/s41467-018-03027-z, 2018.

Ren, Y. G., Grosselin, B., Daele, V., and Mellouki, A.: Investigation of the reaction of ozone with isoprene, methacrolein and methyl vinyl ketone using the HELIOS chamber, Faraday Discuss., 200, 289–311, 2017.

Rollins, A. W., Kiendler-Scharr, A., Fry, J. L., Brauers, T., Brown, S. S., Dorn, H.-P., Dubé, W. P., Fuchs, H., Mensah, A., Mentel, T. F., Rohrer, F., Tillmann, R., Wegener, R., Wooldridge, P. J., and Cohen, R. C.: Isoprene oxidation by nitrate radical: alkyl nitrate and secondary organic aerosol yields, Atmos. Chem. Phys., 9, 6685–6703, https://doi.org/10.5194/acp-9-6685-2009, 2009.

Rudzinski, K. J.: Heterogeneous and Aqueous-Phase Transformations of Isoprene, Springer, Dordrecht, 261–277, https://doi.org/10.1007/1-4020-4232-9_23, 2006.

Stern, J. E., Flagan, R. C., Grosjean, D., and Seinfeld, J. H.: Aerosol Formation And Growth In Atmospheric Aromatic Hydrocarbon Photooxidation, Environ. Sci. Technol., 21, 1224–1231, 1987.

Su, H., Cheng, Y., Zheng, G., Wei, C., Mu, Q., Zheng, B., Wang, Z., Zhang, Q., He, K., and Carmichael, G.: Reactive nitrogen chemistry in aerosol water as a source of sulfate during haze events in China, Sci. Adv., 2, e1601530, https://doi.org/10.1126/sciadv.1601530, 2016.

Su, H., Cheng, Y., and Pöschl, U.: New Multiphase Chemical Processes Influencing Atmospheric Aerosols, Air Quality, and Cli-

mate in the Anthropocene, Accounts Chem. Res., 53, 2034–2043, https://doi.org/10.1021/acs.accounts.0c00246, 2020.

Takekawa, H., Minoura, H., and Yamazaki, S.: Temperature dependence of secondary organic aerosol formation by photo-oxidation of hydrocarbons, Atmos. Environ., 37, 3413–3424, 2003.

Thuner, L. P., Bardini, P., Rea, G. J., and Wenger, J. C.: Kinetics of the gas-phase reactions of OH and NO_3 radicals with dimethylphenols, J. Phys. Chem. A, 108, 11019–11025, 2004.

Tolkacheva, G. A.: Problems of Air Quality in Tashkent City, Springer, Dordrecht, 379–392, https://doi.org/10.1007/1-4020-4232-9_32, 2006.

Turšič, J., Grgić, I., and Podkrajek, B.: Influence of ionic strength on aqueous oxidation of SO_2 catalyzed by manganese, Atmos. Environ., 37, 2589–2595, https://doi.org/10.1016/s1352-2310(03)00215-2, 2003.

Virtanen, A., Joutsensaari, J., Koop, T., Kannosto, J., Yli-Pirila, P., Leskinen, J., Makela, J. M., Holopainen, J. K., Poschl, U., Kulmala, M., Worsnop, D. R., and Laaksonen, A.: An amorphous solid state of biogenic secondary organic aerosol particles, Nature, 467, 824–827, https://doi.org/10.1038/nature09455, 2010.

Wang, B., O'Brien, R. E., Kelly, S. T., Shilling, J. E., Moffet, R. C., Gilles, M. K., and Laskin, A.: Reactivity of liquid and semisolid secondary organic carbon with chloride and nitrate in atmospheric aerosols, J. Phys. Chem. A, 119, 4498–4508, https://doi.org/10.1021/jp510336q, 2015.

Wang, G. H., Zhang, R. Y., Gomez, M. E., Yang, L. X., Zamora, M. L., Hu, M., Lin, Y., Peng, J. F., Guo, S., Meng, J. J., Li, J. J., Cheng, C. L., Hu, T. F., Ren, Y. Q., Wang, Y. S., Gao, J., Cao, J. J., An, Z. S., Zhou, W. J., Li, G. H., Wang, J. Y., Tian, P. F., Marrero-Ortiz, W., Secrest, J., Du, Z. F., Zheng, J., Shang, D. J., Zeng, L. M., Shao, M., Wang, W. G., Huang, Y., Wang, Y., Zhu, Y. J., Li, Y. X., Hu, J. X., Pan, B., Cai, L., Cheng, Y. T., Ji, Y. M., Zhang, F., Rosenfeld, D., Liss, P. S., Duce, R. A., Kolb, C. E., and Molina, M. J.: Persistent sulfate formation from London Fog to Chinese haze, P. Natl. Acad. Sci. USA, 113, 13630–13635, https://doi.org/10.1073/pnas.1616540113, 2016.

Wang, J., Doussin, J. F., Perrier, S., Perraudin, E., Katrib, Y., Pangui, E., and Picquet-Varrault, B.: Design of a new multi-phase experimental simulation chamber for atmospheric photosmog, aerosol and cloud chemistry research, Atmos. Meas. Tech., 4, 2465–2494, https://doi.org/10.5194/amt-4-2465-2011, 2011.

Wang, W. G., Li, K., Zhou, L., Ge, M. F., Hou, S. Q., Tong, S. R., Mu, Y. J., and Jia, L.: Evaluation and Application of Dual-Reactor Chamber for Studying Atmospheric Oxidation Processes and Mechanisms, Acta Phys.-Chim. Sin., 31, 1251–1259, 2015.

Wang, X., Liu, T., Bernard, F., Ding, X., Wen, S., Zhang, Y., Zhang, Z., He, Q., Lü, S., Chen, J., Saunders, S., and Yu, J.: Design and characterization of a smog chamber for studying gas-phase chemical mechanisms and aerosol formation, Atmos. Meas. Tech., 7, 301–313, https://doi.org/10.5194/amt-7-301-2014, 2014.

Warneke, C., de Gouw, J. A., Goldan, P. D., Kuster, W. C., Williams, E. J., Lerner, B. M., Jakoubek, R., Brown, S. S., Stark, H., Aldener, M., Ravishankara, A. R., Roberts, J. M., Marchewka, M., Bertman, S., Sueper, D. T., McKeen, S. A., Meagher, J. F., and Fehsenfeld, F. C.: Comparison of daytime and nighttime oxidation of biogenic and anthropogenic VOCs along the New England coast in summer during New England Air Quality Study 2002, J. Geophys. Res.-Atmos., 109, D10309, https://doi.org/10.1029/2003JD004424, 2004.

Wenger, J. C.: Chamber Studies on the Photolysis of Aldehydes Environmental, Springer, Dordrecht, 111–119, https://doi.org/10.1007/1-4020-4232-9_8, 2006.

White, S., Angove, D., Li, K. W., Campbell, I., Element, A., Halliburton, B., Lavrencic, S., Cameron, D., Jamie, I., and Azzi, M.: Development of a new smog chamber for studying the impact of different UV lamps on SAPRC chemical mechanism predictions and aerosol formation, Environ. Chem., 15, 171–182, 2018.

Wu, S., Lu, Z. F., Hao, J. M., Zhao, Z., Li, J. H., Hideto, T., Hiroaki, M., and Akio, Y.: Construction and characterization of an atmospheric simulation smog chamber, Adv. Atmos. Sci., 24, 250–258, 2007.

Zhang, Y., Sanchez, M. S., Douet, C., Wang, Y., Bateman, A. P., Gong, Z., Kuwata, M., Renbaum-Wolff, L., Sato, B. B., Liu, P. F., Bertram, A. K., Geiger, F. M., and Martin, S. T.: Changing shapes and implied viscosities of suspended submicron particles, Atmos. Chem. Phys., 15, 7819–7829, https://doi.org/10.5194/acp-15-7819-2015, 2015.

Zhang, Y., Chen, Y., Lambe, A. T., Olson, N. E., Lei, Z., Craig, R. L., Zhang, Z., Gold, A., Onasch, T. B., Jayne, J. T., Worsnop, D. R., Gaston, C. J., Thornton, J. A., Vizuete, W., Ault, A. P., and Surratt, J. D.: Effect of the Aerosol-Phase State on Secondary Organic Aerosol Formation from the Reactive Uptake of Isoprene-Derived Epoxydiols (IEPOX), Environ. Sci. Technol. Lett., 5, 167–174, https://doi.org/10.1021/acs.estlett.8b00044, 2018.

Zhang, Y., Chen, Y., Lei, Z., Olson, N. E., Riva, M., Koss, A. R., Zhang, Z., Gold, A., Jayne, J. T., Worsnop, D. R., Onasch, T. B., Kroll, J. H., Turpin, B. J., Ault, A. P., and Surratt, J. D.: Joint Impacts of Acidity and Viscosity on the Formation of Secondary Organic Aerosol from Isoprene Epoxydiols (IEPOX) in Phase Separated Particles, ACS Earth Space Chem., 3, 2646–2658, https://doi.org/10.1021/acsearthspacechem.9b00209, 2019.

Zheng, J., Shi, X., Ma, Y., Ren, X., Jabbour, H., Diao, Y., Wang, W., Ge, Y., Zhang, Y., and Zhu, W.: Contribution of nitrous acid to the atmospheric oxidation capacity in an industrial zone in the Yangtze River Delta region of China, Atmos. Chem. Phys., 20, 5457–5475, https://doi.org/10.5194/acp-20-5457-2020, 2020.

Zhou, S., Hwang, B. C. H., Lakey, P. S. J., Zuend, A., Abbatt, J. P. D., and Shiraiwa, M.: Multiphase reactivity of polycyclic aromatic hydrocarbons is driven by phase separation and diffusion limitations, P. Natl. Acad. Sci. USA, 116, 11658–11663, https://doi.org/10.1073/pnas.1902517116, 2019.

Zielinska, B., Sagebiel, J., Stockwell, W., McDonald, J., Seagrave, J., Wiesen, P., and Wirtz, K.: Investigation of Atmospheric Transformations of Diesel Emissions in the European Photoreactor (EUPHORE), Springer, Dordrecht, 279–284, https://doi.org/10.1007/1-4020-4232-9_24, 2006.

Ziemann, P. J. and Atkinson, R.: Kinetics, products, and mechanisms of secondary organic aerosol formation, Chem. Soc. Rev., 41, 6582–6605, https://doi.org/10.1039/c2cs35122f, 2012.